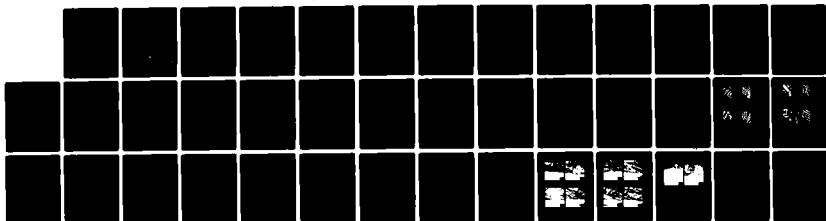AD-A129 811   EFFECT OF MICROSTRUCTURE STRENGTH AND OXYGEN CONTENT ON   1/1
               FATIGUE CRACK GRO..(U) NAVAL RESEARCH LAB WASHINGTON DC
               G R YODER ET AL. 17 JUN 83 NRL-MR-5091
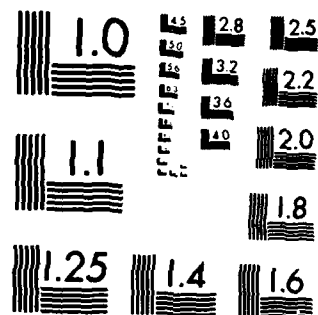
UNCLASSIFIED   F/G 11/6   NL

MICROCOPY RESOLUTION TEST CHART
NATIONAL BUREAU OF STANDARDS-1963-A

Effect of Microstructure, Strength and Oxygen Content on Fatigue Crack Growth Rate of Ti-4.5Al-5.0Mo-1.5Cr (CORONA 5)

G. R. YODER, F. H. FROES,* AND D. EYLON**

Mechanics of Materials Branch
Material Science and Technology Division

*Air Force Wright Aeronautical Laboratories
Wright-Patterson AFB, OH 45433

**Metcut-Materials Research Group
Wright-Patterson AFB, OH 45433

June 17, 1983

NAVAL RESEARCH LABORATORY
Washington, D.C.

REPORT DOCUMENTATION PAGE		READ INSTRUCTIONS BEFORE COMPLETING FORM
1. REPORT NUMBER NRL Memorandum Report 5091	2. GOVT ACCESSION NO. AD-A129 811	3. RECIPIENT'S CATALOG NUMBER
4. TITLE (and Subtitle) EFFECT OF MICROSTRUCTURE, STRENGTH AND OXYGEN CONTENT ON FATIGUE CRACK GROWTH RATE OF Ti-4.5Al-5.0Mo-1.5Cr (CORONA 5)		5. TYPE OF REPORT & PERIOD COVERED Final report on one phase of a continuing NRL problem.
		6. PERFORMING ORG. REPORT NUMBER
7. AUTHOR(s) G.R. Yoder, F.H. Froes,* and D. Eylon**		8. CONTRACT OR GRANT NUMBER(s) Air Force Contracts F33615-79-C-5152 and F33615-82-C-5078
9. PERFORMING ORGANIZATION NAME AND ADDRESS Naval Research Lab., Washington, DC 20375 Air Force Wright Aeronautical Lab., WPAFB, OH 45433 Metcut-Materials Res. Group, WPAFB, OH 45433		10. PROGRAM ELEMENT, PROJECT, TASK AREA & WORK UNIT NUMBERS 61153N-22; RR022-01-48; 63-1079-0-3; 63-1553-0-3
11. CONTROLLING OFFICE NAME AND ADDRESS Naval Air Systems Command Office of Naval Research Washington, DC 20361 Arlington, VA 22217		12. REPORT DATE June 17, 1983
		13. NUMBER OF PAGES 39
14. MONITORING AGENCY NAME & ADDRESS(if different from Controlling Office)		15. SECURITY CLASS. (of this report) UNCLASSIFIED
		15a. DECLASSIFICATION/DOWNGRADING SCHEDULE

16. DISTRIBUTION STATEMENT (of this Report)

Approved for public release; distribution unlimited.

17. DISTRIBUTION STATEMENT (of the abstract entered in Block 20, if different from Report)

19. KEY WORDS (Continue on reverse side if necessary and identify by block number)

Fatigue (materials)	Microstructure
Fatigue crack growth	Oxygen content
Titanium alloys	Strength
CORONA 5	

20. ABSTRACT (Continue on reverse side if necessary and identify by block number)

Fatigue crack growth rate behavior in CORONA 5, an alloy developed for applications requiring high fracture toughness, has been examined for eight material conditions. These conditions were designed to give differences in microstructure, strength level (825-1100 MPa [120-160 ksi]), and oxygen content (0.100-0.174 wt-pct), in such a manner that the separate effects of these variables could be defined. For all eight conditions, fatigue crack growth rates (da/dN) are virtually indistinguishable over the full

(Continues)

DD FORM 1473   EDITION OF 1 NOV 68 IS OBSOLETE
1 JAN 73
S/N 0102-014-6601

20. ABSTRACT (Continued)

spectrum of stress-intensity range (ΔK) examined, viz. 8 to 40 MPa$\sqrt{m}$ (7 to 36 ksi$\sqrt{in}$). Con-comitantly, it is noted that over the sizeable solution annealing range studied (830—945 C [1525-1675 F]), the primary α-phase morphology was substantially invariant. Each da/dN curve exhibits a bilinear form with a transition point (ΔK_T) between 16 and 19 MPa$\sqrt{m}$ (15 and 17 ksi$\sqrt{in}$). A change in microfractographic appearance occurs at ΔK_T^-, as extensive secondary cracking along α/β interfaces is observed at all hypertransitional levels of ΔK, but not for $\Delta K < \Delta K_T^-$. For each material condition, the mean length of primary α platelets is approximately the same as the cyclic plastic zone size at ΔK_T^-. Accordingly, locations of ΔK_T^- (and their similarity for the different material conditions) are rationalized in conformance with a cyclic plastic zone model of fatigue crack growth. Finally, the difference in behavior of CORONA 5, as compared to con-ventional α/β alloys such as Ti-6Al-4V, is rationalized in terms of crack path behavior.

CONTENTS

EFFECT OF MICROSTRUCTURE, STRENGTH AND OXYGEN CONTENT ON FATIGUE

CRACK GROWTH RATE OF Ti-4.5Al-5.0Mo-1.5Cr (CORONA 5)

G. R. Yoder*, F. H. Froes** and D. Eylon***

INTRODUCTION

During the past decade, increased emphasis has been placed on the fracture mechanics characteristics of metallic materials for use in high performance aerospace systems. While fracture toughness is a requirement which has been demanded for applications such as the B1 bomber, an even more critical parameter in lifing a part is the fatigue crack growth rate (FCGR). As such, this mechanical property has received extensive attention and many data on various materials have been developed. However, in many cases, these data have not indicated exactly how various material characteristics, such as strength level, microstructure and oxygen level separately influence the FCGR. It was the goal of the present work to separate out the effect of these various factors for a new fracture resistant titanium alloy, Ti-4.5Al-5.0Mo-1.5Cr (CORONA 5****) [1-6].

To separate out these effects, a matrix of conditions was evaluated (Table 1). The effect of oxygen level was studied at two levels (0.100 and 0.174 wt pct) while keeping the microstructure constant. Constant micro-

---

structure was attained by solution treating at ~30°C (55°F) and ~90°C (160°F)
below the beta transus temperature for both oxygen levels. This was then
followed by aging treatments at lower temperatures designed to give the de-
sired strength levels. The solution treatment temperature was considered
critical, as previous work had indicated that the coarse alpha formed at this
temperature controlled the fracture path rather than the fine alpha resulting
from subsequent aging [7]. The goal strength levels were 825 MPa (120 ksi)
and 960 MPa (140 ksi) UTS for the low oxygen material and 960 MPa (140 ksi)
and 1100 MPa (160 ksi) for the high oxygen material. The two materials at
the 960 MPa (140 ksi) level would allow direct comparision of oxygen
strengthening versus alpha phase dispersion strengthening, while the two
strength levels for a constant oxygen content would allow the influence of
change in strength level by alpha phase dispersion variations to be defined
for both oxygen levels. Thus the effects of oxygen level and strengthening
due to the dispersion of fine alpha phase should be determined unambiguously.
Additionally, the influence of the coarse alpha phase produced at the solu-
tion treatment temperature should be defined, for both oxygen levels and at
constant strength level (produced by the fine alpha precipitation).

MATERIAL AND METHODS

Melting and Processing

The low oxygen material (subsequently referred to by the letter L) was
melted as a 225kg (500 lb) ingot [8]. It was subsequently rolled from above
the beta transus temperature (915°C [1675°F]) out of a 970°C (1775°F) furnace
from 10cm (4 inches) down to 3.8cm (1.5 inches) with a 20-25% reduction per
pass. The high oxygen material (subsequently referred to by the letter H)
was melted as a 2180kg (4800 lb) ingot [9]. It was then also rolled from

above the beta transus temperature (940°C [1725°F]) out of a 980°C (1800°F) furnace from 7.6cm (3 inches) down to 3.2cm (1.25 inches) again with 20-25% reduction per pass. The higher furnace temperature was used to normalize for the higher beta transus temperature of the higher oxygen material.

Heat Treatment

Heat treatment of the two plates was carried out in the beta region to ensure complete solution of the alpha phase followed by water quenching. This ensured that subsequent heat treatment in the alpha-beta region would produce lenticular alpha [5,6], for maximum fatigue crack growth rate resistance.

The low oxygen material was heat-treated at 830°C (1525°F) and 885°C (1625°F) and was aged at the temperatures and times shown in Table I to achieve the desired microstructure/strength combinations based on preliminary heat treatment studies. The high oxygen material was solution-treated at higher temperatures (845°C [1550°F] and 970°C [1675°F]) than the corresponding low oxygen material to adjust for the effect of higher oxygen level on the beta transus temperature and, hence, proportion of primary alpha phase (Table I). All solution treatments and subsequent aging were carried out in an air furnace followed by an air-cool.

Chemical Analysis

The chemical analysis of Groups L and H are indicated in Table II. It should be noted that the oxygen level of the H material (0.174%) is 74% higher than that for the L material (0.100%).

Tensile Tests

For each of the eight material conditions, two cylindrical tensile specimens of L orientation [10] were machined with a 6.25mm (0.25 inch) diameter

3

and a gage length of 25.4mm (1 inch). Specimens were tested in accordance with ASTM E8-81 [11] with a rate of stressing, $\dot{\sigma}$ = 172 MPa min^{-1} (25 ksi min^{-1}).

Fatigue Crack Growth Rate Determination

Heat-treated specimen blanks from the plate materials were machined into compact-type (CT) specimens of an LT crack orientation [10], a thickness (B) of 25.4mm (1 inch), a width (W) of 49.8mm (1.96 inch) and a half-height-to-width ratio (h/W) of 0.60. These and other specimen dimensions are illustrated in Fig. 1. The stress-intensity (K) for this specimen is given by the following expression [12]:

$$K = \frac{P}{B\sqrt{W}} \frac{(2 + \alpha)}{(1-\alpha)^{3/2}} \; (0.886 + 4.64 \; \alpha - 13.32 \; \alpha^2 + 14.72 \; \alpha^3 - 5.6 \; \alpha^4) \qquad (1)$$

where, P is the load and α is the normalized crack length (a/W). Specimens were cyclically stressed with a haversine loadform of constant amplitude, a stress ratio ($\sigma_{min}/\sigma_{max}$) of R = 0.10 and a frequency (ν) of 5Hz in ambient air, using closed-loop servohydraulic loading equipment.

The precision measurement technique described by Yoder, Cooley and Crooker [13] was employed to determine fatigue crack growth rates (da/dN) in accordance with ASTM E647-81 [12]. Crack length (a) was determined as a function of elapsed cycles (N) from measurements of crack-mouth-opening displacement (CMOD), using the calibration equations of Saxena and Hudak (14):

$$a/W = 1.0010 - 4.6695 \; U + 18.460 \; U^2 - 236.82 \; U^3$$
$$+ 1214.9 \; U^4 - 2143.6 \; U^5 \qquad (2)$$

where,

$$U = \cfrac{1}{\left[\cfrac{EB(CMOD)}{P}\right]^{1/2} + 1} \qquad (3)$$

and E is Young's modulus.

Resistance to fatigue crack growth was measured over a nominal spectrum of stress-intensity-range (ΔK) levels from about 8 to 40 MPa√m (7 to 36 ksi√in). However, specimens of the CORONA 5 alloy, regardless of the particular material condition, tended to exhibit an uncommon propensity toward development of skewed crack fronts - which rendered data in several instances to be invalid.* Consequently, even though two and, in most cases, three individual specimens were studied for each material condition, it was not possible in all cases to determine valid da/dN data over the full spectrum of intended ΔK levels. In the results which follow, only the fully valid data are reported, except for two material conditions (H3 and L1) where a few data are included that appear to be only marginally invalid - as denoted by flagged data points, and the case of material condition L4 where virtually all of the data appeared invalid.

Fractographic Techniques

To provide information on the relationships between microstructure and fracture features of the various material conditions, the fracture surfaces of FCGR specimens from each group were examined. The specimens were sectioned along the centerline of the fracture surface on a plane perpendicular to

---

* Crack fronts were skewed across the specimen thickness, as opposed to departure from the Mode I plane of symmetry. To straighten such crack fronts, it was helpful in many instances to substantially increase the ΔK level used in precracking (by 2 or 3 fold) - which, of course, necessitated subsequent and significant load shedding. Hu [15] has observed similar behavior in an HT-9 steel.

the fracture plane. The sectioned plane was, then, polished and etched using conventional titanium metallographic practices. The metallographic mount material was removed and the cleaned surfaces were viewed in the SEM at an angle which allowed the fracture topography and the polished and etched surfaces to be observed simultaneously.

RESULTS

Microstructure

The microstructures of all low oxygen (L) conditions are shown in Figs. 2a through d and the microstructures of the high oxygen (H) conditions in Figs. 3a through d. It should be noted that the four conditions solution treated at a high temperature and subsequently aged at high temperatures (L1,L2,H1,H2) (730°C and 790°C [1346°F and 1454°F]) did not produce any fine precipitation at this latter temperature (cf. inserts in Figs. 2a, b and 3a, b). It is probable that the low driving force for further alpha rejection coupled with the relatively high diffusion rate resulted only in a coarsening of the coarse primary alpha laths. In contrast, the other four conditions (L3,L4, H3,H4) all resulted in a fine alpha dispersion after the low temperature aging (cf. inserts in Figs. 2c, d and 3c, d). The volume fraction of the primary alpha was determined by point counting using 2000X and 5000X SEM photomicrographs and 2.5mm (0.1 inch) and 5.0mm (0.2 inch) grids at 0°, 30° and 330° orientations. Determinations of α-platelet lengths are also shown in Table III. These estimates of true platelet length assume the adjustment factor of 1.68 employed by Thompson and Backofen [16], applied to the quantitative metallographic measurements. The results are listed in Table III.

Tensile Results

The tensile properties are shown in Table IV as a function of heat treatment for both the high and low oxygen plate materials.

6

Fatigue Crack Growth Rate

For each of the eight material conditions, fatigue crack growth rates (da/dN) are displayed as a function of stress-intensity range (ΔK) in the logarithmic plots of Figs. 4-11. Examination of these plots reveals that the growth rate data in each case exhibit a bilinear form [17] as anticipated, with a transition point ΔK_T in the vicinity of 16 to 19 MPa$\sqrt{m}$ (15 to 17 ksi$\sqrt{in}$).*

To facilitate comparison of the growth-rate behavior for the different cases, a summary plot is shown in Fig. 12, composed of data trend lines (solid) for all eight conditions except L4.** This figure shows that the fatigue crack growth rates are remarkably similar for the different material conditions - over the whole spectrum of ΔK levels examined. ⋅ ι fact, the growth rate curves are so alike that it was not quite feasible ᵤᵤ superpose yet distinguish all the individual data trend lines in this ᵗration.) For example, in the hypertransitional region at $\Delta K = 25$ MPa$\sqrt{m}$ (23 ksi$\sqrt{in}$), the da/dN values are all within 15 percent of each other. In the hypotransitional region, e.g., at $\Delta K = 10$ MPa$\sqrt{m}$ (9 ksi$\sqrt{in}$), da/dN values for the different material conditions are all within 50 percent of each other.

From this comparative plot, it appears that neither increased oxygen content nor strength level, per se, affects the fatigue crack growth resistance in the CORONA 5 alloy.

Also, in Fig. 12, data from the present study are compared in relation to the upper and lower bounds (cf. dashed lines labeled "UB" and "LB", respec-

---

* Region III behavior [18, 19] is not addressed in the present paper; rather, attention is focused on power-law behavior [20] as manifest in bilinear form.

** In the case of L4, virtually all of the data in Fig. 7 are invalid - as noted earlier, and consequently, must be discounted as to significance.

tively) of fatigue crack growth rate data from an earlier, preliminary study of CORONA 5 alloy [9]. Over most of the spectrum of ΔK levels examined in the present study, da/dN values appear to cluster much closer to the lower bound values observed in the prior work. Consequently, fatigue crack growth behavior of the CORONA 5 alloy observed in the present study compares much more favorably with that of conventional alpha/beta alloys (e.g., Ti-6Al-4V) than apparent from prior upper bound data.

Fractography

Since the corresponding conditions in the low and high oxygen groups were very similar (Figs. 2 and 3), the resulting fracture features were also very similar. Therefore, we have elected to show only fractographs of one oxygen level group for each one of the four microstructural conditions. Microstructure/fracture mode relationships for conditions L1, L2, H3 and H4 are shown in Figs. 13-16, respectively. Examination of the specimens revealed a change in fracture mode associated with the hypotransitional and hypertransitional sections of individual da/dN curves, common to all material conditions used in this work. Specifically, it was found that for all values of ΔK in excess of the transitional level (ΔK_T), extensive secondary cracking occurred at α/β interfaces. By contrast, for all values of $\Delta K < \Delta K_T$, this interfacial cracking virtually disappeared. This contrast is readily apparent from the pair of fractographs shown in each figure for the (a) hypotransitional and (b) hypertransitional cases. (Fractographs displayed were taken near either $\Delta K = 10$ or 30 MPa$\sqrt{m}$ [9 or 27 ksi$\sqrt{in}$]).

A view of the interfacial cracking at higher magnification is shown in Fig. 17(a). In Fig. 17(b), an example of a transcolony cracking mode is shown, as observed only on rare occasion in CORONA 5, in the hypotransitional region. In conventional α/β titanium alloys such as Ti-6Al-4V, this type of

8

cracking is, by contrast, very commonly observed in the hypotransitional region.

DISCUSSION

The results presented in Table IV indicate that the strength levels for all eight conditions came close to goal levels. However, the quantitative metallographic results in Table III show that the distribution of coarse primary alpha did not vary substantially between the eight conditions evaluated. From a practical view-point, this is a positive feature since it reflects a lack of sensitivity of microstructure to heat-treatment, implying that unduly tight quality control is not necessary. However, from the view-point of the present study, it means that the coarse primary alpha dispersion was removed as a variable, leaving oxygen level and strength level.

The CORONA 5 fatigue crack growth results show an interesting behavior compared to that of conventional α/β alloys such as Ti-6Al-4V. In Fig. 18, the summary of da/dN data trend lines for the CORONA 5 conditions (from Fig. 12) is compared to the databand for conventional α/β alloys reported in Ref. 21. Clearly, both the hypotransitional and hypertransitional slopes for the CORONA 5 conditions appear less steep than for the conventional α/β alloys. This contrast in behavior follows from the opposing propensities, in CORONA 5 vs. alloys such as Ti-6Al-4V, for secondary cracking (or crack bifurcation) to occur in the respective limbs of the da/dN curve. Specifically, the crack branching occurs in the hypotransitional limb in the case of Ti-6Al-4V [22,23] but is virtually absent in the CORONA 5 - with these propensities for secondary cracking reversed in the hypertransitional limb of the da/dN curves. Beevers [24] predicted such a situation some years ago, which can be readily understood with reference to Fig. 19. Fig. 19(a) shows schematically that if crack branching occurs in the hypotransitional limb, the slope is

increased. On the other hand, if the crack branching occurs in the hyper-transitional limb - cf. Fig. 19(b), then the slope should decrease relative to that for the nonbifurcated case. Consequently, it is not surprising that at low values of ΔK, resistance ⌐˙ CORONA 5 to fatigue crack growth tends to be somewhat inferior to that of conventional α/β alloys, but superior at high values of ΔK. (Additionally, it is noted that the higher fracture toughness of CORONA 5 serves to extend region II fatigue crack growth behavior to high-er levels of ΔK - compared to conventional α/β alloys, and thus to even fur-ther enhance the superior fatigue crack growth resistance of CORONA 5.)

Of course, the location of the transition points, ΔK_T, has a bearing on the ordering of fatigue crack growth rates for different materials at a spe-cific level of ΔK. In the case of conventional α/β alloys, positions of ΔK_T have been ascribed to the development of a critical size of the cyclic plas-tic zone ($r_y{}^c$), viz. that of the effective α-grain size ($\bar{\ell}$) [17,21,23]. As a consequence, values of ΔK_T have been predicted according to:

$$\Delta K_T = 5.5 \; \sigma_{ys} \sqrt{\bar{\ell}} \tag{4}$$

where σ_{ys} is the yield stress and $\bar{\ell}$ is - in the more general sense, the mean free path between barriers to slip band transmission.

In CORONA 5 values of ΔK_T are evidently linked in a critical way to the incidence of interfacial secondary cracking (for $\Delta K > \Delta K_T$). Inasmuch as pri-mary α-platelets constitute little more than 50% of the CORONA 5 micro-structures - as indicated in Table III, these individual platelets are sur-rounded with very sizable regions of β-phase as compared to the typical case of Ti-6Al-4V or Ti-8Al-1Mo-1V (where phase equilibrium dictates that the amount of β-phase may be insufficient to provide even a continuous film about primary α grains). Since the elastic (Young's) modulus is significantly less

10

for β-phase than α-phase – though the strength levels may be roughly equivalent (presuming estimates of Smelser, Swedlow and Williams [25]), then in response to applied loading, the yield point of the α-phase should be exceeded first (with the β-phase remaining elastic). However, the elastic constraint to which the α-phase is thereby subjected may well serve to generate high stresses at the α/β interface, as suggested in the modeling of Smelser, Swedlow and Williams [25]. In the present work, there is evidence to suggest that such stresses may exceed a critical level sufficient to generate interfacial cracks, when the cyclic plastic zone size (r_y^c) exceeds the length dimension of the α-platelets $(\bar{\ell}_L)$. Values of $\bar{\ell}_L$, from Table III, are compared (for the eight material conditions) in Table V to the sizes of r_y^c at the transition point [17],

$$[r_y^c]_T = 0.033 \left(\frac{\Delta K_T}{\sigma_{ys}}\right)^2 . \tag{5}$$

The correspondence is reasonable. This evidence is also consistent with the observation that ΔK_T is relatively similar for the eight conditions. Observed values of ΔK_T, from Figs. 4-11 are compared to values computed from Eqn. (4), using values of $\bar{\ell}_L$. Again, the agreement is reasonable.

CONCLUSIONS

The present study of fatigue crack growth rate behavior in CORONA 5 showed that:

1. Oxygen content (in the range of 0.100 – 0.174 wt pct) or strength level (in the range of 825 – 1100 MPa [120 – 160 ksi] UTS), per se, does not affect the fatigue crack growth rate. At the 960 MPa (140 ksi) UTS strength level, the fatigue crack growth is the same irrespective of whether this strength is developed by alpha precipitation or oxygen level.

11

2. Within the solution annealing range studied in the present program (830° − 915°C [1525° − 1675°F]) the coarse primary alpha dispersion showed little variation. This is a positive practical feature from a quality control standpoint, but it did mean that a study of this variable was not possible in the present program.

3. For each of the eight material conditions examined, fatigue crack growth rates are remarkably similar over the full spectrum of ΔK levels studied. Each growth-rate curve exhibits a bilinear form with a transition point (ΔK_T) between 16 and 19 MPa$\sqrt{m}$ (15 and 17 ksi$\sqrt{in}$).

4. A change in fractographic appearance occurs at ΔK_T, as extensive secondary cracking along α/β interfaces is observed at all hypertransitional levels of ΔK, but not for $\Delta K < \Delta K_T$. Thus, the propensities for secondary cracking are opposite to trends reported for Ti-6Al-4V. This observation helps to explain why CORONA 5, relative to conventional α/β alloys such as Ti-6Al-4V, tends to exhibit inferior fatigue crack growth resistance at lower ΔK levels, but superior resistance at high levels of ΔK.

5. For each material condition, the mean length of primary α platelets is approximately the same as the cyclic plastic zone size at ΔK_T. Accordingly, positions of the respective da/dN curves and their similarity for the eight material conditions are rationalized in conformance with a cyclic plastic zone model of fatigue crack growth.

this work. In addition, helpful discussions with Dr. V. Mahajan, Mr. M. E. Rosenblum, and Mr. C. F. Yolton are appreciated. The experimental assistance of Mr. G. Lovell, Mr. C. Cooke and Mr. A. Houston is gratefully acknowledged. The work was carried out, in part, under Air Force Contracts F33615-79-C-5152 and F33615-82-C-5078.

REFERENCES

1. R. G. Berryman, J. C. Chesnutt, F. H. Froes, and J. C. Williams: _Journal of Aircraft_, December 1977, Vol. 14, No. 12, p. 1182.

2. R. G. Berryman, J. C. Chesnutt, and F. H. Froes: _Metal Progress_, Vol. 112, No. 8, December 1977, p. 40.

3. J. C. Williams, F. H. Froes, J. C. Chesnutt, C. G. Rhodes, and R. G. Berryman: _Toughness and Fracture Behavior of Titanium_, ASTM STP 651, pp. 64-114, American Society for Testing and Materials, Philadelphia, PA, 1978.

4. G. R. Keller, J. C. Chesnutt, W. T. Highberger, C. G. Rhodes, and F. H. Froes: _Titanium '80_, edited by H. Kimura and O. Izumi, TMS-AIME Publications, Vol. 2, Warrendale, PA, 1980, pp. 1209-1220.

5. F. H. Froes, V. C. Petersen, P. F. Malone, R. G. Berryman, J. C. Chesnutt, C. G. Rhodes, and J. C. Williams: ICM-11, 1976, p. 2009.

6. F. H. Froes and W. T. Highberger: _Journal of Metals_, Vol. 32, No. 5, May 1980, p. 57.

7. J. P. Hirth and F. H. Froes: _Met. Trans._, Vol. 8A, July 1977, p. 1165.

8. R. G. Berryman, F. H. Froes, J. C. Chesnutt, C. G. Rhodes, J. C. Williams and R. F. Malone: Rockwell International Corp. Report TFD-74-657 to Naval Air Systems Command, July 1974.

9. G. R. Keller, J. C. Chesnutt, F. H. Froes and C. G. Rhodes: Rockwell International Corp. Report NA-78-917 to Naval Air Systems Command, December 1978.

10. R. J. Goode, <u>Mater. Res. Stand.</u>, 1972, Vol. 12, No. 9 p. 31.

11. E8-81, "Standard Methods of Tension Testing of Metallic Materials", <u>1981 Annual Book of ASTM Standards</u>, Part 10, ASTM, Philadelphia, PA, 1981, pp. 197-217.

12. E647-81, "Standard Test Method for Constant-Load Amplitude Fatigue Crack Growth Rates Above 10^{-8}m/cycle", <u>1981 Annual Book of ASTM Standards</u>, Part 10, ASTM, Philadelphia, PA, 1981, pp. 765-783.

13. G. R. Yoder, L. A. Cooley and T. W. Crooker: <u>Fatigue Crack Growth Measurement and Data Analysis</u>, S. J. Hudak, Jr. and R. J. Bucci, eds., ASTM STP 738, ASTM, Philadelphia, PA, 1981, pp. 85-102.

14. A. Saxena and S. J. Hudak, Jr.: <u>Inter. J. Fracture</u>, 1978, Vol. 14, pp. 453-468.

15. W. L. Hu: Westinghouse Hanford Company, Richland, WA, personal communication, 1982.

16. A. W. Thompson and W. A. Backofen: <u>Acta Met.</u>, 1971, Vol. 19, pp. 597-606.

17. G. R. Yoder, L. A. Cooley and T. W. Crooker: <u>Titanium '80</u>, H. Kimura and O. Izumi, eds., TMS-AIME, Vol. 3, Warrendale, PA, 1980, pp. 1865-1874.

18. R. W. Hertzberg: <u>Deformation and Fracture Mechanics of Engineering Materials</u>, John Wiley and Sons, New York, 1976, p. 486.

19. S. T. Rolfe and J. M. Barsom: <u>Fracture and Fatigue Control in Structures</u>, Prentice-Hall, Englewood Cliffs, NJ, 1977, p. 235.

20. P. C. Paris and F. Erdogan: <u>Trans. ASME, J. Basic Eng.</u>, 1963, Series D, Vol. 85, pp. 528-533.

21. G. R. Yoder, L. A. Cooley and T. W. Crooker: <u>Trans. ASME, J. Engng. Mater. Tech.</u>, 1979, Series H, Vol. 101, pp. 86-90.

22. P. E. Irving and C. J. Beevers: *Mater. Sci. Eng.*, 1974, Vol. 14, pp. 229-38.

23. G. R. Yoder, L. A. Cooley and T. W. Crooker: *Met. Trans. A*, 1977, Vol. 8A, pp. 1737-1743.

24. C. J. Beevers: University of Birmingham, Great Britain, personal communication, 1978.

25. R. E. Smelser, J. L. Swedlow and J. C. Williams: *Toughness and Fracture Behavior of Titanium*, ASTM STP 651, pp. 200-215, American Society for Testing and Materials, Philadelphia, PA, 1978.

TABLE I

Heat-Treat Conditions

Material Condition	Oxygen Level	Strength[a] Goal	Solution Treatment[b] °C(°F)/hr.	Aging Treatment[b] °C(°F)/hr.
L1	Low	LO	885(1625)/1	790(1450)/8
L2	Low	LO	830(1525)/4	730(1350)/8
L3	Low	INT	885(1625)/1	540(1000)/16
L4	Low	INT	830(1525)/4	495(925)/24
H1	High	INT	915(1675)/1	790(1450)/8
H2	High	INT	845(1550)/4	730(1350)/8
H3	High	HI	915(1675)/1	595(1100)/8
H4	High	HI	845(1550)/4	540(1000)/16

[a] LO = Low: 825MPa (120ksi) UTS
INT = Intermediate: 960MPa (140ksi) UTS
HI = High: 1100MPa (160ksi) UTS.

[b] Followed by air-cool (AC).

TABLE II

Chemical Analysis[a] of Alloy Compositions Used in the Work (wt.pct.)

Cond.	Al	Mo	Cr	Fe	C	O	N	H
L	4.0	5.1	1.3	.06	.01	.100	.004	.0021
H	4.5	4.5	1.6	.30	.01	.174	.010	.0024

[a] Average of eight values for interstitials.

TABLE III

Primary Alpha Phase in the Various Conditions

Material Condition	Alpha Volume Fraction (pct)	Length of platelets, $\bar{\ell}_L$ (µm)
L1	50.3	12.4
L2	59.0	12.2
L3	56.7	12.2
L4	53.4	10.5
H1	60.3	9.4
H2	59.3	11.0
H3	51.7	11.6
H4	55.3	12.1

TABLE IV

Tensile Properties

Material Condition	Goal UTS MPa	(ksi)	UTS MPa	(ksi)	0.2% YS MPa	(ksi)	EL 4D (%)
Low Oxygen							
L1	825	(120)	850	(123)	760	(110)	22
L2	825	(120)	820	(119)	745	(108)	22
L3	960	(140)	925	(134)	800	(116)	15
L4	960	(140)	985	(143)	815	(118)	15
High Oxygen							
H1	960	(140)	945	(137)	890	(129)	22
H2	960	(140)	955	(138)	890	(129)	21
H3	1100	(160)	1055	(153)	955	(139)	15
H4	1100	(160)	1100	(160)	985	(143)	15

TABLE V

Analysis of Transitional FCGR Behavior

Material Condition	α-Platelet Length, $\bar{\ell}_L$ (μm)	Transitional Cyclic Plastic Zone Size $[r_y^c]_T$ (μm)	Observed Transition Point, ΔK_T (MPa√m)	Computed Transition Point, ΔK_T (MPa√m)
L1	12.4	15.6	16.5	14.7
L2	12.2	15.2	16.0	14.3
L3	12.2	12.7	15.7	15.4
L4	10.5	(14.1)*	(16.8)*	14.5
H1	9.4	11.9	16.9	15.0
H2	11.0	12.1	17.0	16.2
H3	11.6	9.5	16.2	17.9
H4	12.1	11.8	18.6	18.8

* Data for condition L4 must be discounted as to significance, owing to invalidity noted earlier.
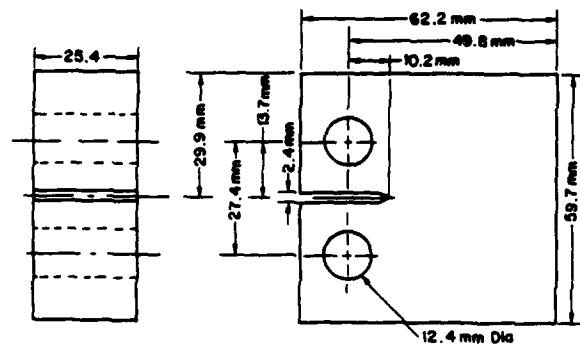
Fig. 1 – Geometry of fatigue crack growth specimen.
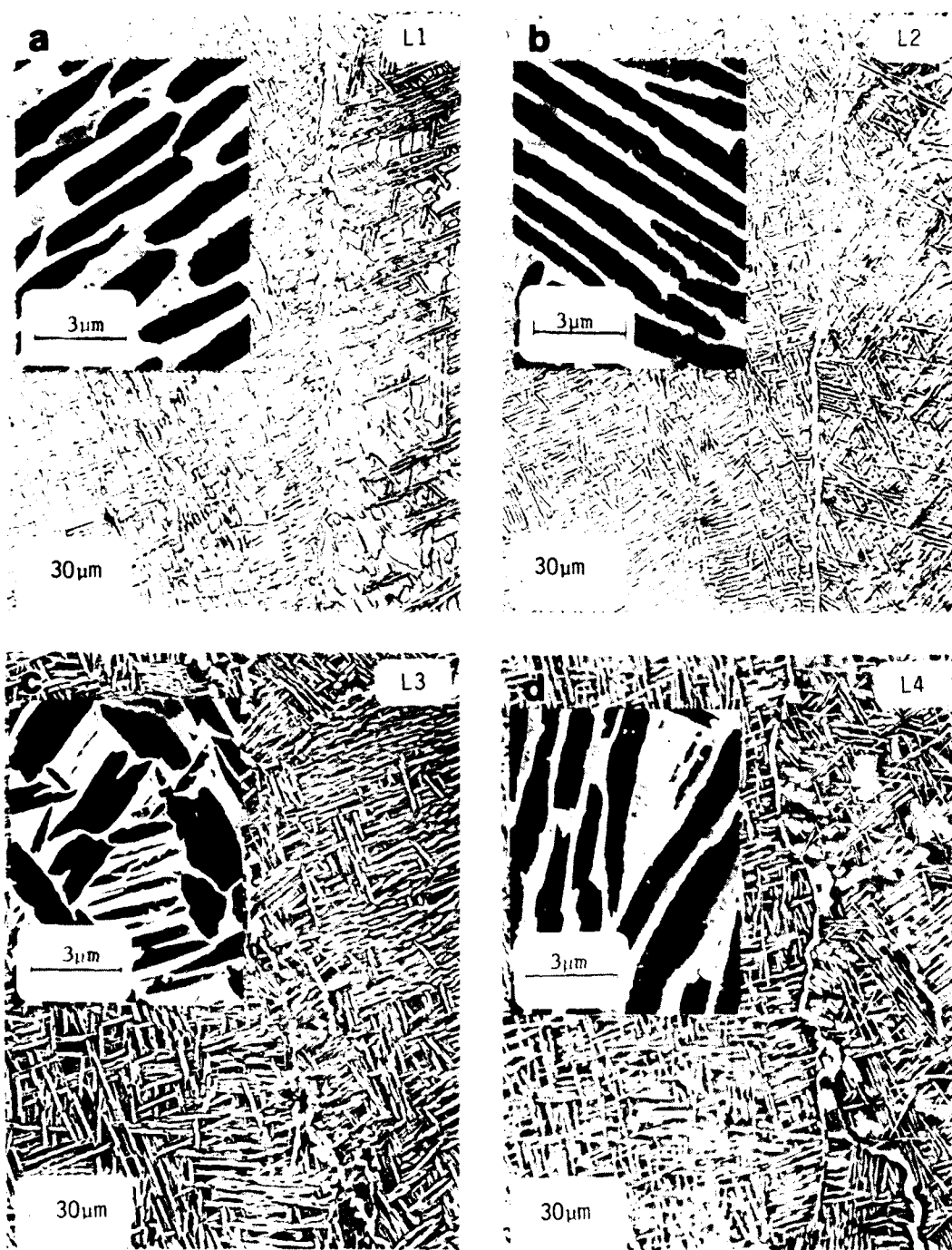
Fig. 2 – Optical microscopy microstructure of low oxygen conditions (primary alpha is the lighter phase). Higher magnifications by SEM secondary electron image are shown in the inserts (primary alpha is the darker phase).

21
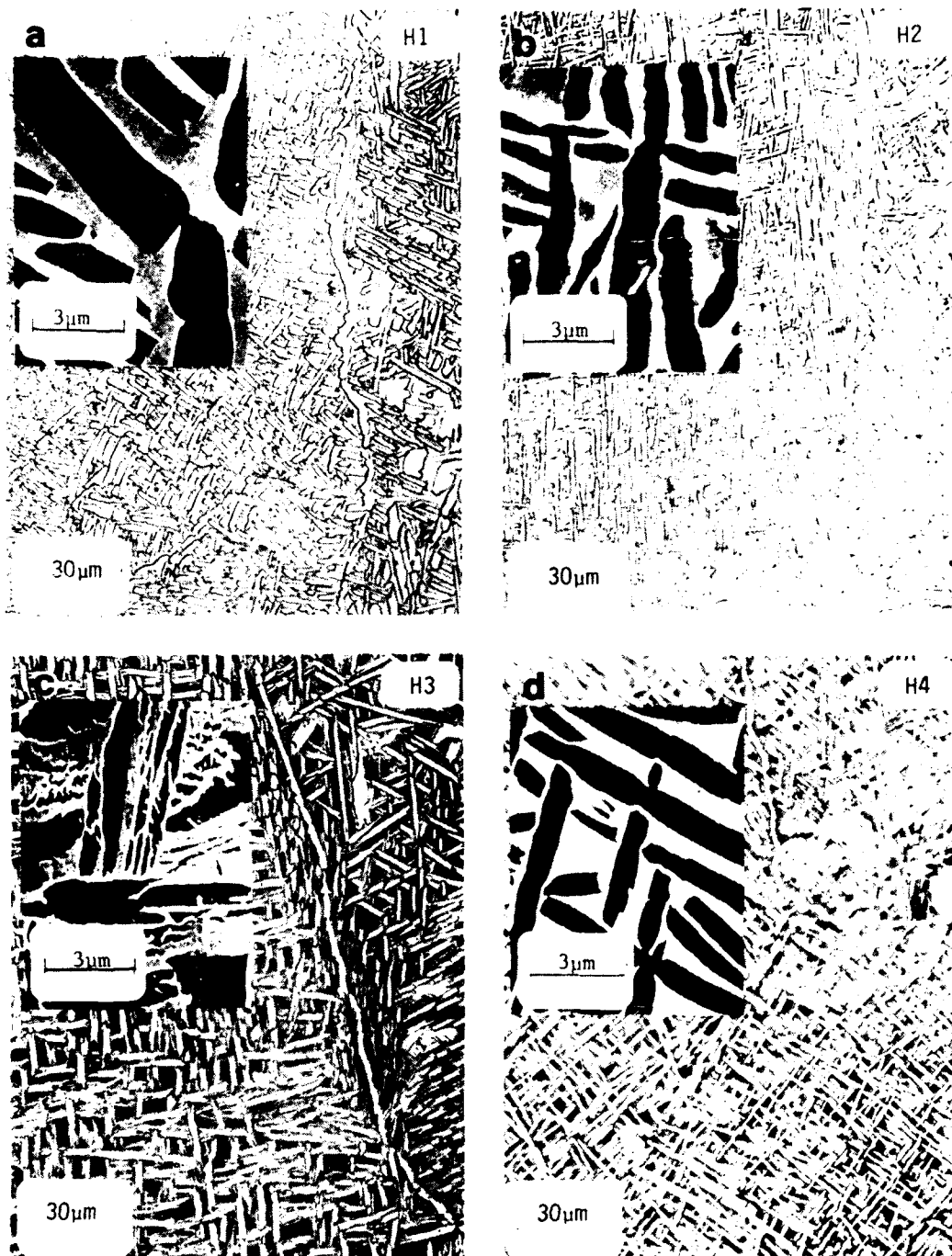
Fig. 3 – Optical microscopy of high oxygen conditions (primary alpha is the
lighter phase). Higher magnifications by SEM secondary electron image
are shown in the inserts (primary alpha is the darker phase).

22
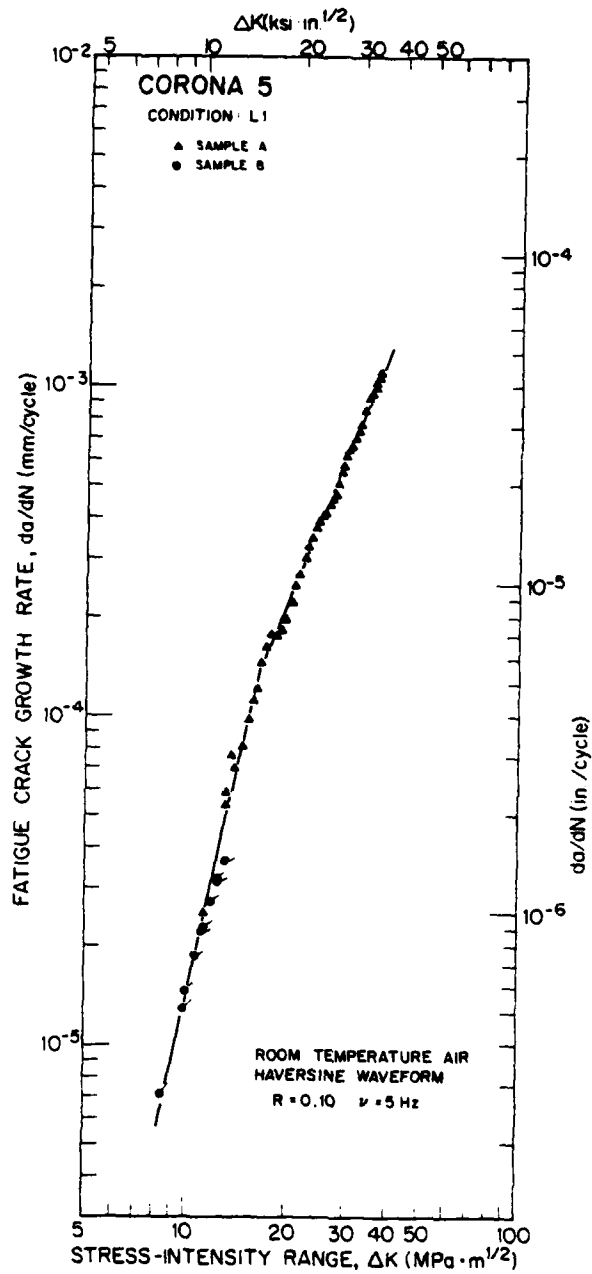
Fig. 4 - Fatigue crack growth rates in CORONA 5, condition L1

23
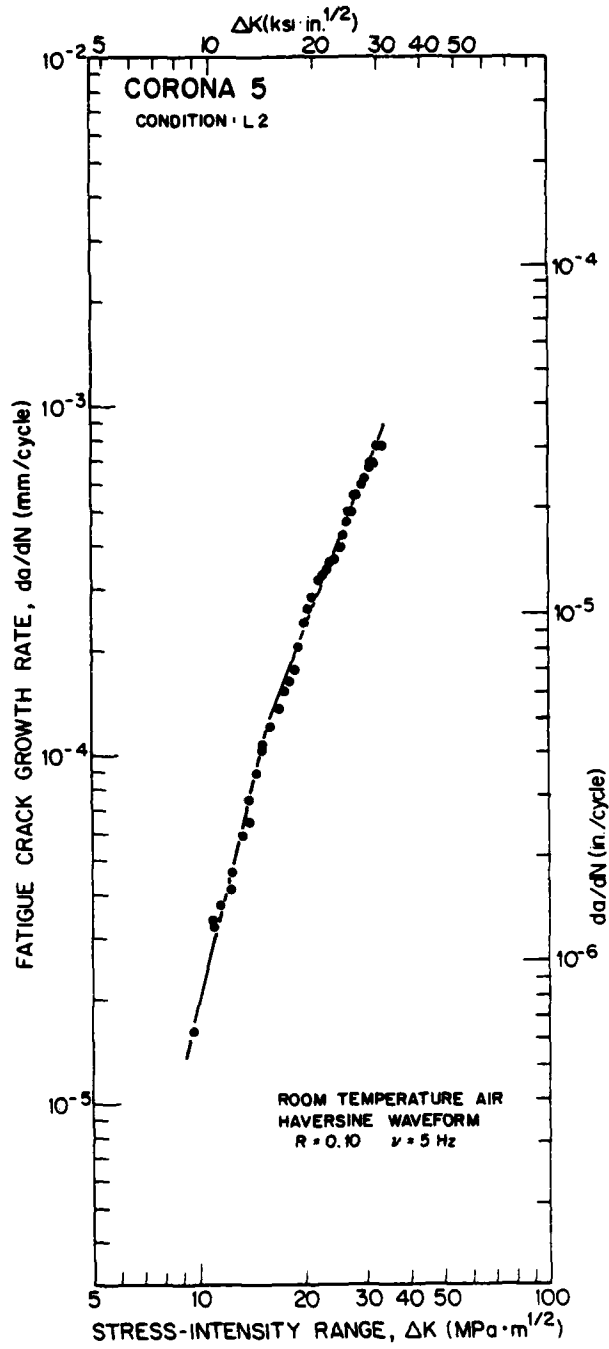
Fig. 5 — Fatigue crack growth rates in CORONA 5, condition L2
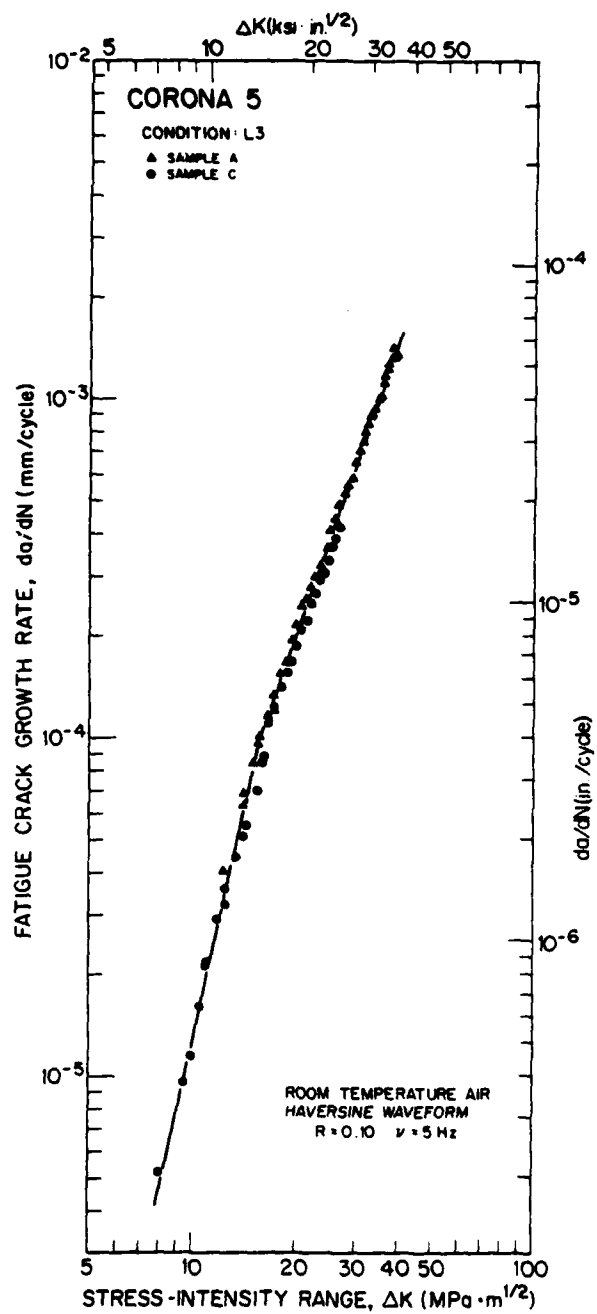
Fig. 6 - Fatigue crack growth rates in CORONA 5, condition L3
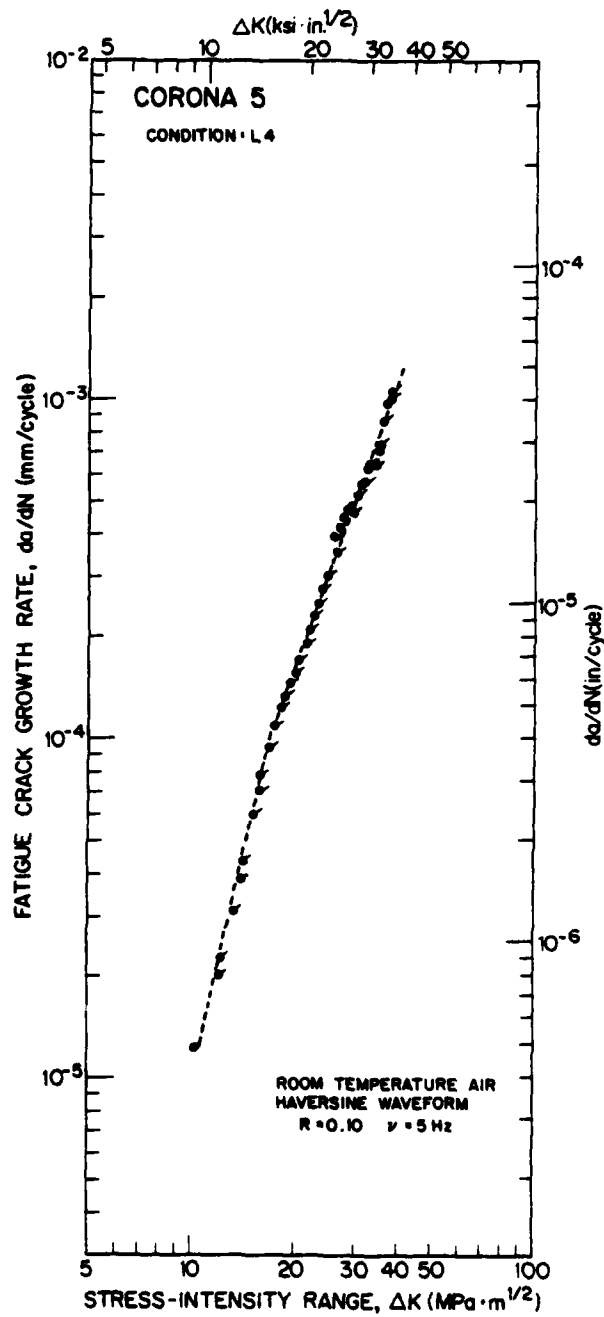
Fig. 7 — Fatigue crack growth rates in CORONA 5, condition L4
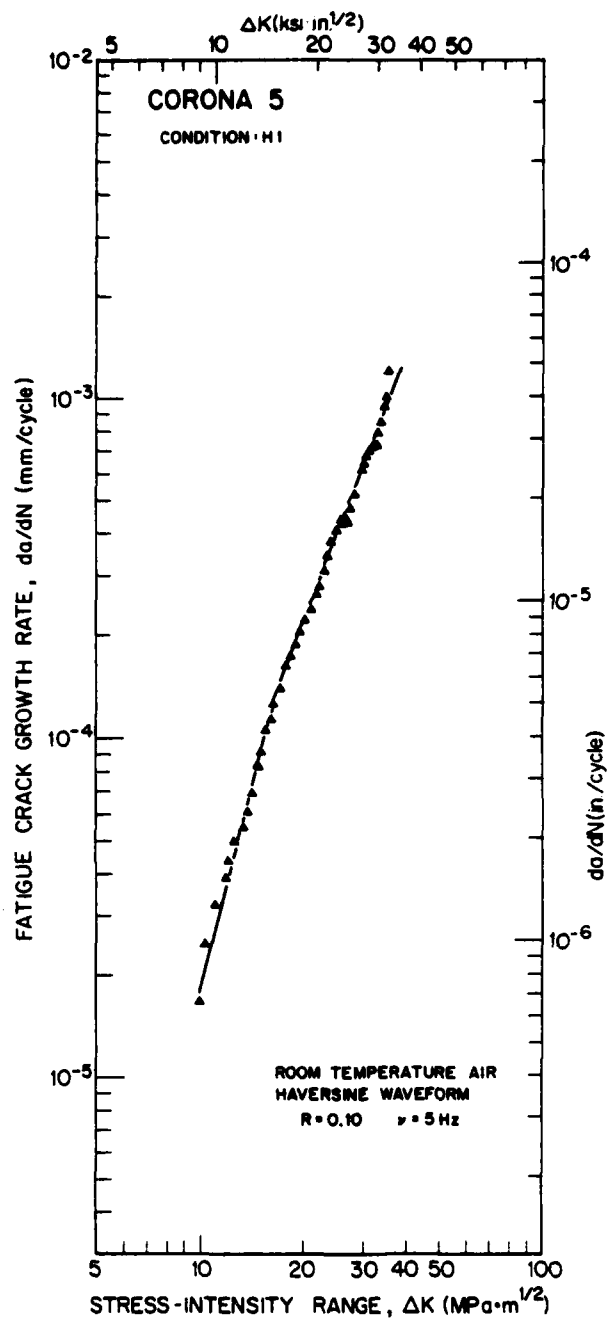
Fig. 8 – Fatigue crack growth rates in CORONA 5, condition H1

Fig. 9 – Fatigue crack growth rates in CORONA 5, condition H2

ΔK(ksi in^{1/2})

CORONA 5

CONDITION: H3

▲ SAMPLE A
● SAMPLE B

FATIGUE CRACK GROWTH RATE, da/dN (mm/cycle)

da/dN (in/cycle)

ROOM TEMPERATURE AIR
HAVERSINE WAVEFORM
R = 0.10   ν = 5 Hz
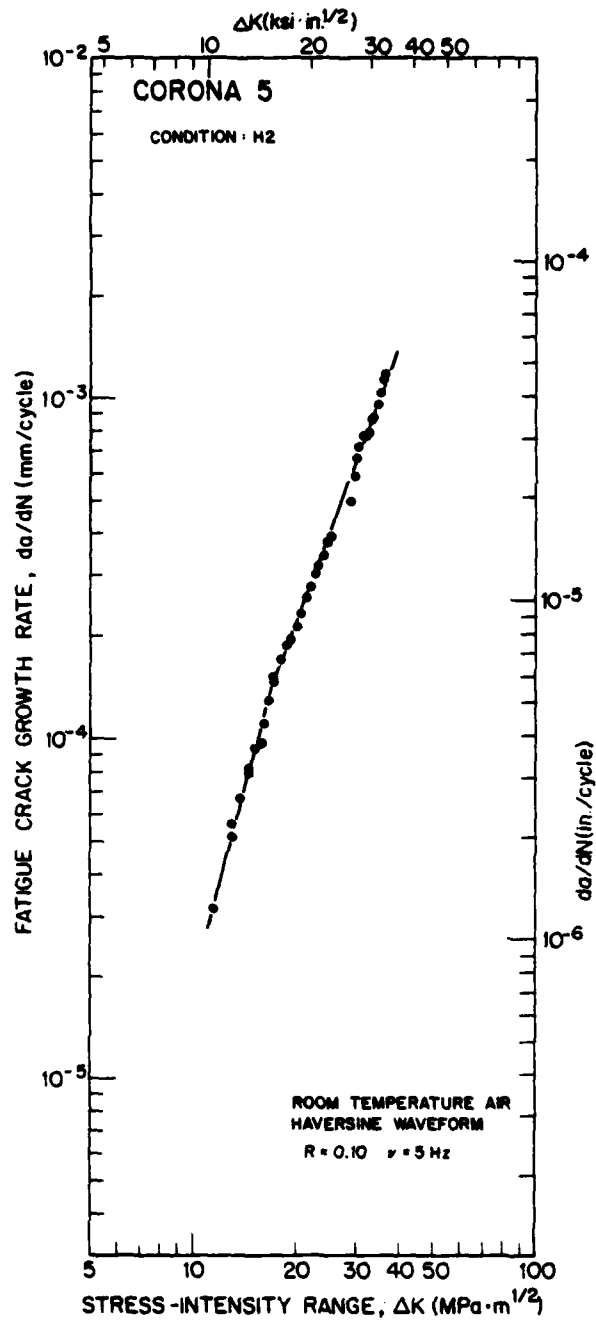
STRESS-INTENSITY RANGE, ΔK (MPa·m^{1/2})
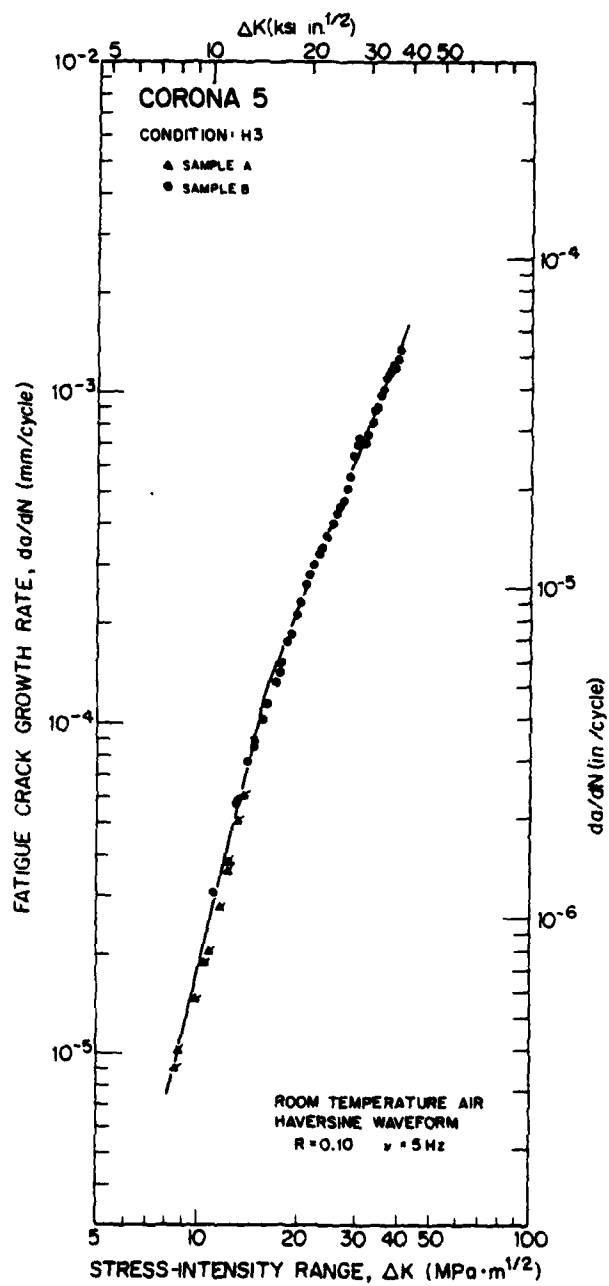
Fig. 10 – Fatigue crack growth rates in CORONA 5, condition H3
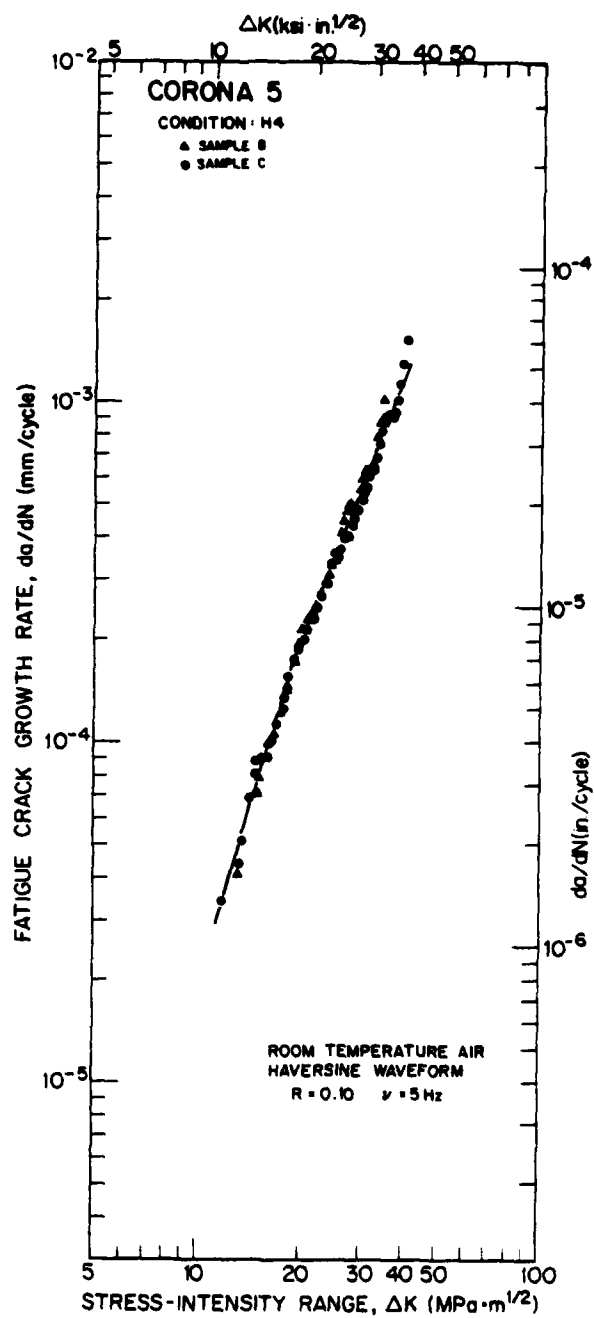
Fig. 11 – Fatigue crack growth rates in CORONA 5, condition H4
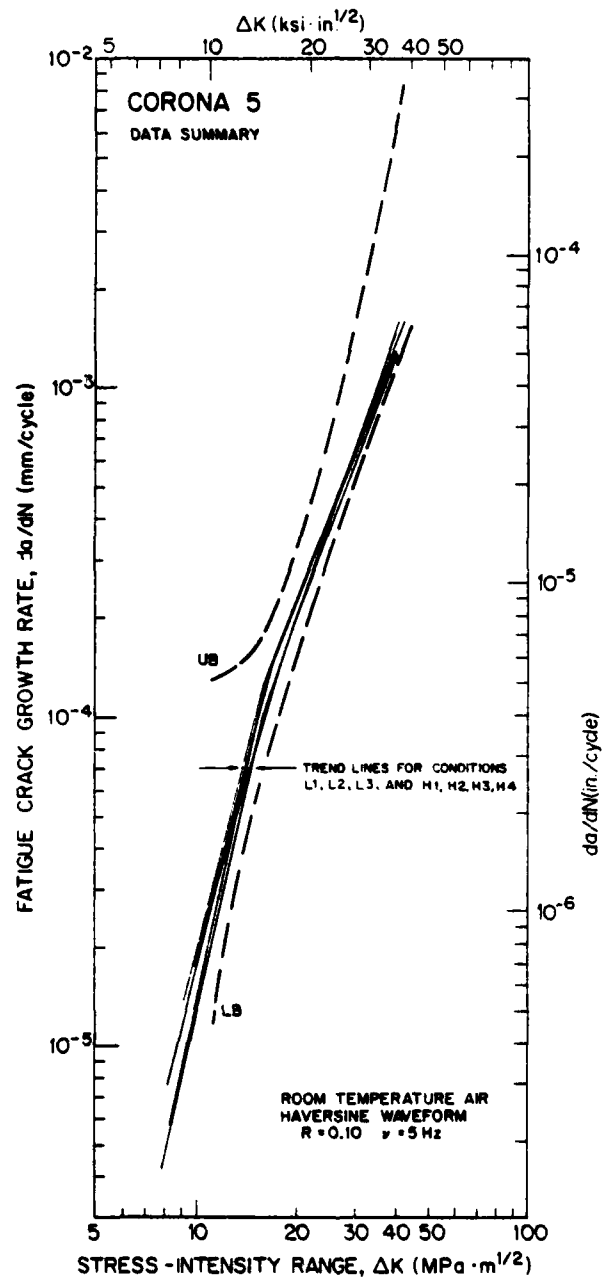
Fig. 12 – Summary plot of fatigue crack growth rates in CORONA 5 alloy
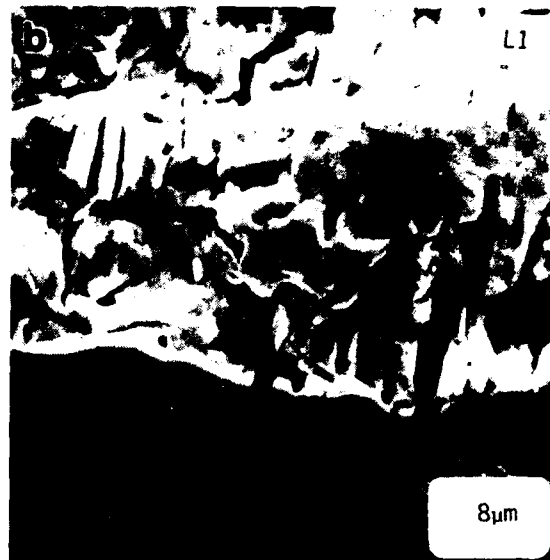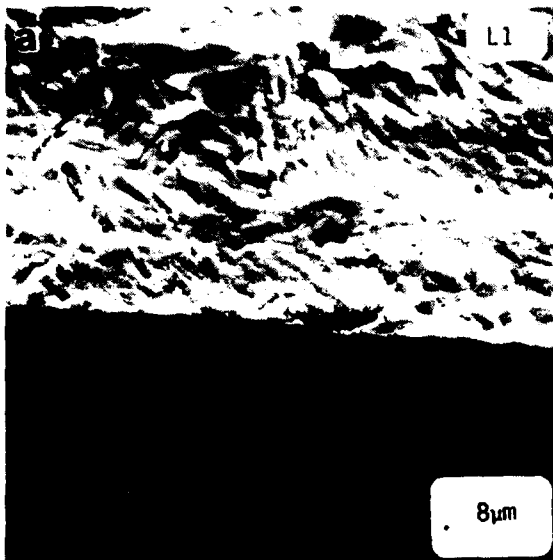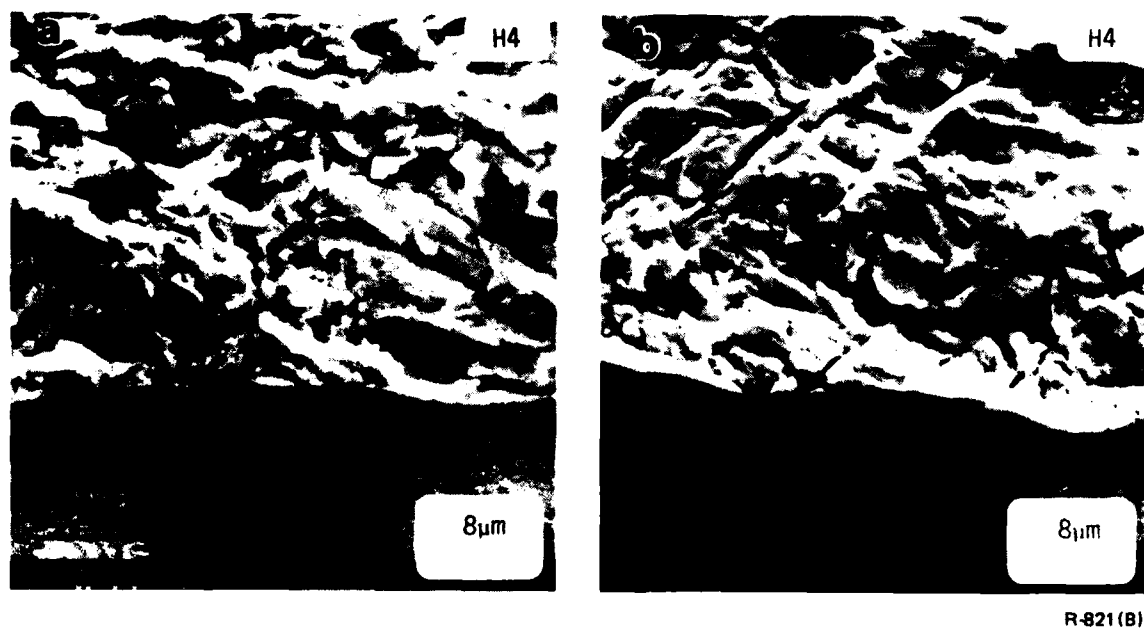
R-822(A)

Fig. 13 – Precision sectioning SEM micrographs for (a) hypotransitional, and
(b) hypertransitional FCGR behavior for condition L1
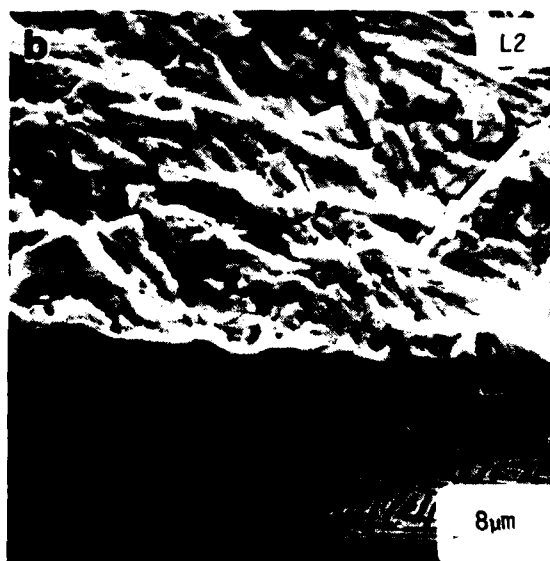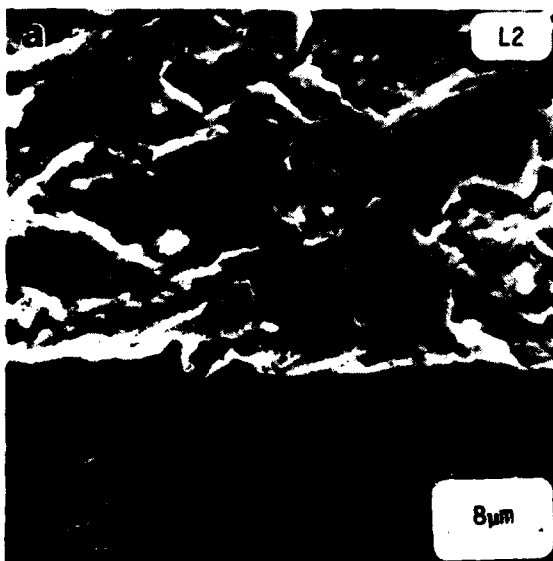
R-822(B)
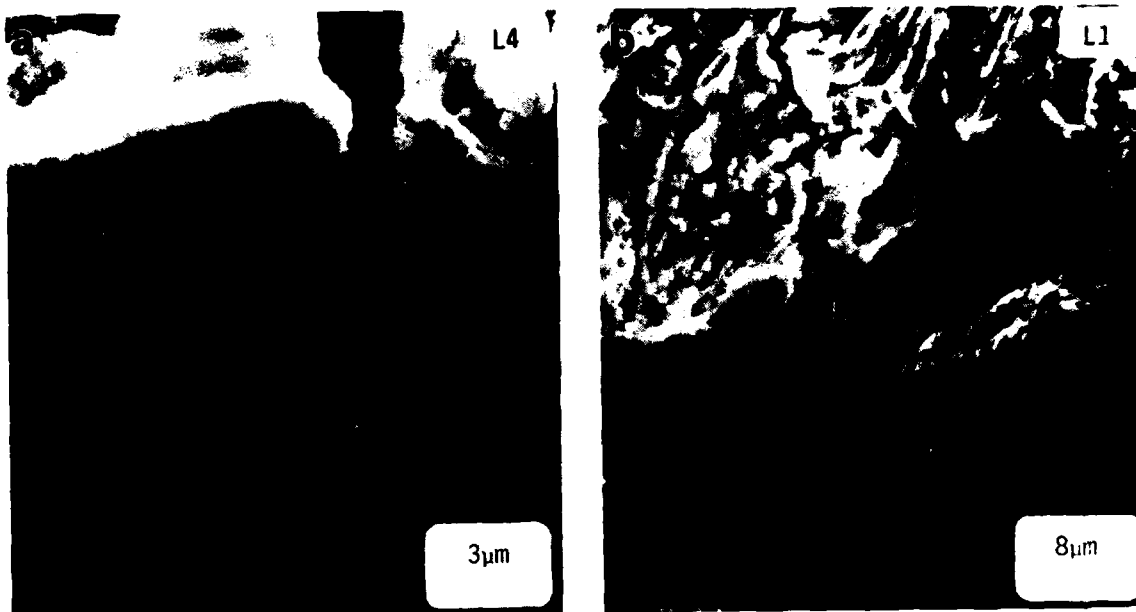
Fig. 14 – Precision sectioning SEM micrographs for (a) hypotransitional, and
(b) hypertransitional FCGR behavior for condition L2
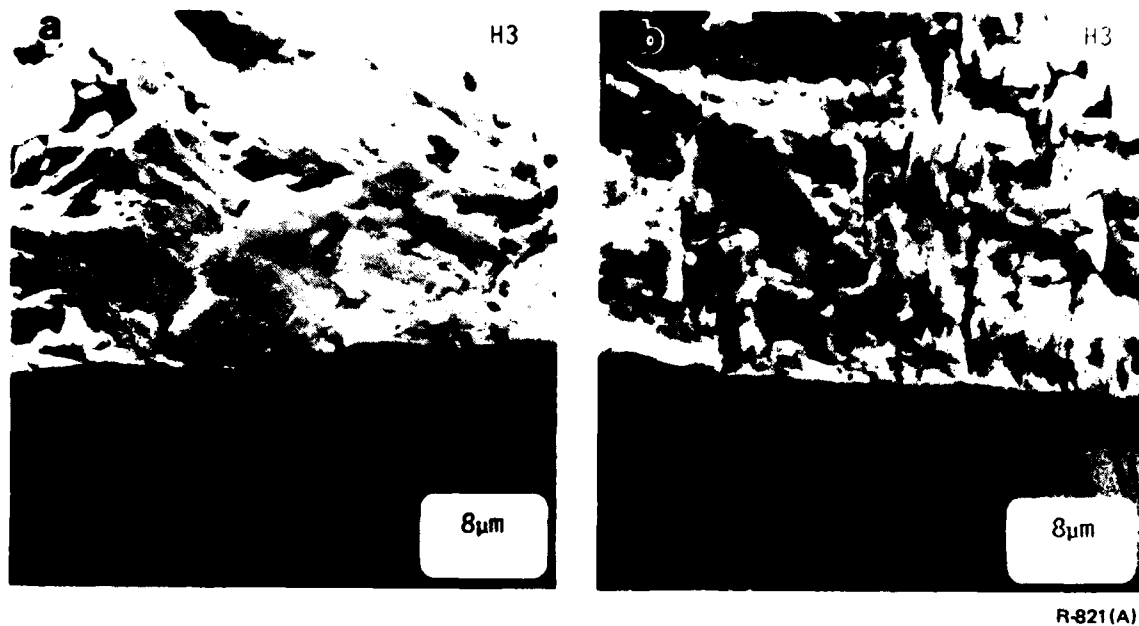
Fig. 15 – Precision sectioning SEM micrographs for (a) hypotransitional, and
(b) hypertransitional FCGR behavior for condition H3

Fig. 16 – Precision sectioning SEM micrographs for (a) hypotransitional, and
(b) hypertransitional FCGR behavior for condition H4

33

Fig. 17 — Precision sectioning SEM micrographs for (a) secondary, α/β interfacial cracking at higher magnification, and (b) rare instance of transcolony cracking mode
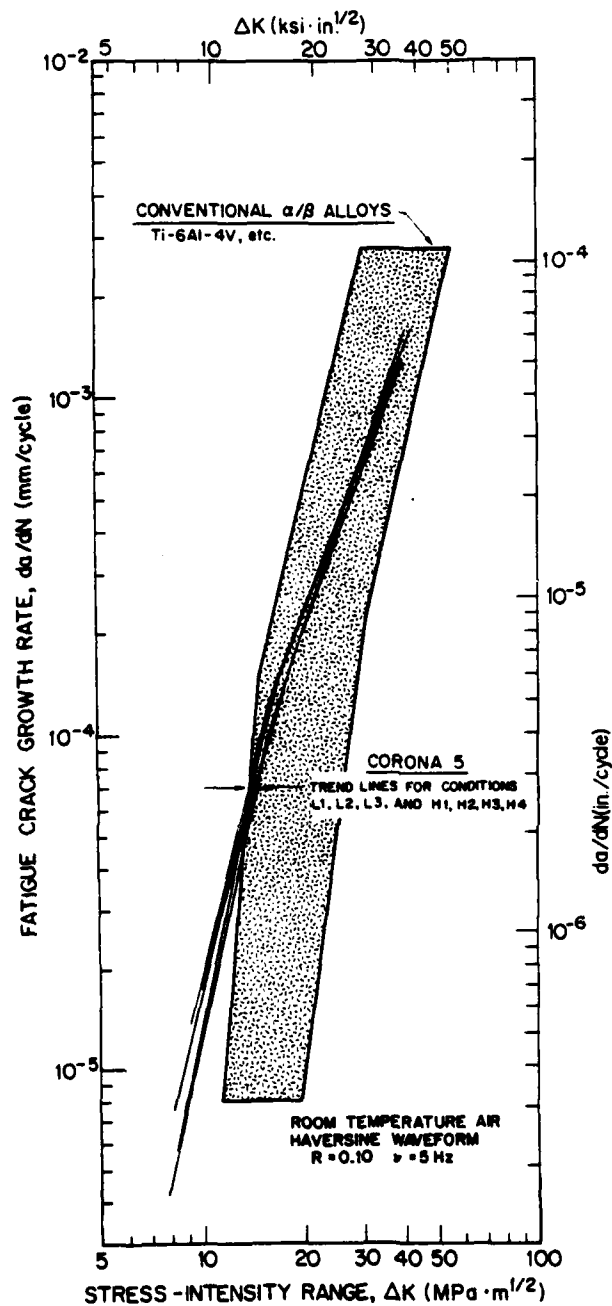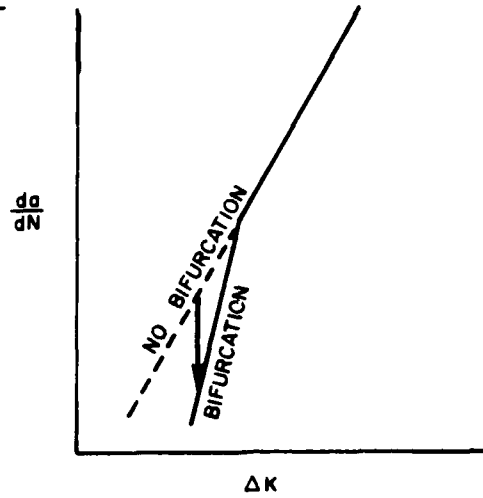
34

Fig. 18 — Comparison of FCGR summary for CORONA 5 conditions, from Fig. 12, to
databand for conventional α/β alloys reported in Ref. 21
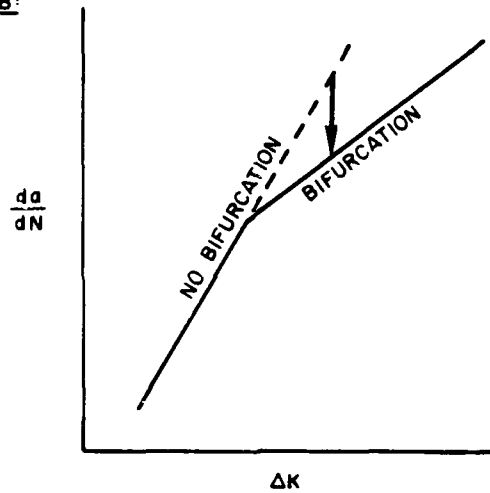
35

CASE A:

CASE B:

Fig. 19 — Effect of crack branching on development of transition in FCGR behavior. Bifurcation in (a) lower limb causes increase in slope; in (b) upper limb causes decrease in slope. In both cases, the occurrence of bifurcation serves to reduce growth rates (da/dN) from what they would otherwise be with no bifurcation (cf. arrows)

36